Environmental Research 298 (2026) 124254

Contents lists available at ScienceDirect

Environmental Research

journal homepage: www.elsevier.com/locate/envres

Assessing green space exposure: From traditional metrics to the Green Exposure Index (GEI) with application to a Northern Italy residential dataset

Niccolò Martini [a,*], Francesca Despini [a], Tommaso Filippini [b,c], Marco Vinceti [b,d], Sergio Teggi [a], Sofia Costanzini [e]

[a] Department of Engineering 'Enzo Ferrari', University of Modena and Reggio Emilia, Modena, Italy
[b] Environmental, Genetic and Nutritional Epidemiology Research Center (CREAGEN), Department of Biomedical, Metabolic and Neural Sciences, University of Modena and Reggio Emilia, Modena, Italy
[c] School of Public Health, University of California Berkeley, Berkeley, CA, USA
[d] Department of Epidemiology, Boston University School of Public Health, Boston, MA, USA
[e] Green Office, Technical Building, Facility Management and Sustainability, University of Modena and Reggio Emilia, Italy

ARTICLE INFO

Keywords:
Green exposure index
NDVI
Landsat imagery
Green accessibility
Multivariate analysis
Urban green space

ABSTRACT

Urban green areas contribute to healthier cities by improving air quality, promoting physical activity and social cohesion, and mitigating the urban heat island effect. However, assessing exposure to green spaces remains a key methodological challenge in epidemiologic research. In this study, we compared traditional green space indices and developed a composite Green Exposure Index (GEI) integrating vegetation cover, density and accessibility to improve exposure assessment. We applied this new index in a population based amyotrophic lateral sclerosis (ALS) case-control dataset from a Northern Italy community. The GEI consists of three components: NDVI, the Green Coverage Ratio and an accessibility index defined for this application. We computed these components for all residential locations across an 8400 km^2 domain from 1985 to 2020. Seasonal NDVI better captured vegetation patterns than annual values, and spatial aggregation restricted to vegetated areas reduced the overestimation associated with circular buffers. The GEI was evaluated under three illustrative weighting scenarios, which produced substantial differences in exposure classification and confirmed that metric choice strongly influences results. In our case study, the equally weighted GEI3 placed 79.7% of the population in the intermediate Mildly Exposed and Exposed categories, resulting in a balanced distribution better suited for epidemiologic analysis. Analysis of GEI time series revealed green space exposure changes from 1985 to 2020, identifying areas characterized by urbanization or green redevelopment. Findings from this case study show the added value of composite indices like the GEI for characterizing green space exposure and capturing long-term dynamics in vegetation and land use, with applications in epidemiology and urban planning.

1. Introduction

Exposure to green spaces has recently emerged as a factor of considerable interest in epidemiological research, due to its dual potential benefits for both physical and mental health. Urban greenery is increasingly recognized as a key element in the design of healthy and sustainable cities, where accessible and high-quality green spaces play an essential role in supporting human well-being and mitigating environmental health inequalities (Ashinze et al., 2024; Kruize et al., 2019). Green areas in urban environments can improve air quality and have been linked to lower stress levels, increased physical activity, and enhanced social cohesion, ultimately contributing to a reduced risk of several chronic diseases (Bagheri et al., 2021; Clark et al., 2025; Gascon et al., 2016; Jones et al., 2025; Kwon et al., 2025; Newton et al., 2026; Slawsky et al., 2022; Soncini et al., 2025; Yuchi et al., 2020). Measuring environmental exposure, however, remains challenging: common GIS-based proximity methods offer practicality and reproducibility, while more complex models can provide more accurate estimates and influence the reliability of epidemiologic findings (Costanzini et al., 2018; Teggi et al., 2018).

* Corresponding author. Department of Engineering 'Enzo Ferrari', University of Modena and Reggio Emilia, Via Vivarelli 10, 41125, Modena, Italy.
E-mail address: niccolo.martini@unimore.it (N. Martini).

https://doi.org/10.1016/j.envres.2026.124254
Received 7 November 2025; Received in revised form 27 February 2026; Accepted 10 March 2026
Available online 11 March 2026

Accurate, comparable, and multidimensional exposure metrics represent a necessary preliminary step for understanding whether and how exposure to green spaces affects health across different populations and contexts. Several approaches have been proposed to evaluate and quantify green spaces. Vegetation indices from satellite images map green areas and capture vegetation density and health (Bannari et al., 1995; Fong et al., 2018; Gascon et al., 2016; Tucker, 1979; Yan et al., 2025). Land cover-based indices quantify the proportion of green spaces. Accessibility-based indices focus on how easily individuals can reach green spaces, often estimated through network-based distances or walking-time thresholds (Kabisch and Haase, 2014; Kwan and Weber, 2003; Villanueva-Durbán et al., 2025), aligning with the "15-min city" paradigm (Barbosa et al., 2007; Moreno et al., 2021). Differences among these approaches may substantially affect exposure assessments: because each method emphasizes distinct aspects of greenery (e.g., density, surface coverage, or accessibility), they can produce markedly different exposure values and, consequently, influence observed relationships with health outcomes (Dadvand et al., 2014; Labib et al., 2020). This aspect underscores the importance of developing metrics that integrate multiple dimensions of green space.

To assess methodological differences among greenness metrics, we used a real-world case study consisting of a population sample of the Emilia-Romagna region, Northern Italy, from a previous population-based study investigating environmental risk factors for the neurodegenerative disease amyotrophic lateral sclerosis (Fiore et al., 2020; Vinceti et al., 2017a, 2017b). This dataset was used exclusively as a set of residential locations that provides a realistic spatial distribution for exposure assessment, with no distinction made between cases and controls. The large size of this dataset, combined with the characteristics of the territory, makes this setting particularly suitable for evaluating methodological differences among exposure indicators. The Emilia-Romagna region is highly heterogeneous, encompassing historic urban centers, suburban residential areas, agricultural land, and urban parks. This heterogeneity produces marked spatial differences in green space exposure, which highlight the limitations in traditional exposure metrics that rely on a single dimension of greenness.

Therefore, the present study aims to compare and evaluate commonly used green exposure metrics, including satellite-derived vegetation indices, land use classifications, and accessibility measures, and to develop a novel composite metric, the Green Exposure Index (GEI), that integrates multiple and complementary dimensions of green space exposure. In addition, we performed supplementary analyses, including principal component analysis (PCA) (Hotelling, 1933; Jolliffe and Cadima, 2016), to explore long-term spatial patterns and the temporal evolution of the GEI in the study area.

2. Methods

2.1. Study area and data sources

Following the approval of the Modena Hospital Ethics Committee (approval no. 80.11 on May 26, 2011), we used a dataset including 2434 residences of ALS cases and matched controls (Fiore et al., 2020; Vinceti et al., 2017a, 2017b) in the provinces of Modena, Parma, and Reggio Emilia, Emilia-Romagna region, Northern Italy (Fig. S1). This represents one of the most densely populated and industrialized areas in Europe, characterized by poor air quality due to its location within the Po Valley, an area with limited atmospheric dispersion (Costanzini et al., 2024; European Environment Agency (EEA), 2023, European Topic Centre on Human Health and the Environment (ETC-HE), 2024). These features make it a relevant case study for investigating environmental exposures in epidemiologic studies (Costanzini et al., 2018).

We derived residential green space indices of study participants related to the vegetation biomass from satellite imagery captured by the Landsat satellite series (Roy et al., 2014; U.S. Geological Survey (USGS), 2019a, U.S. Geological Survey (USGS), 2019b; Wulder et al., 2019). In particular, we used Landsat 5 TM, Landsat 7 ETM+, and Landsat 8 OLI to provide coverage from 1985 to 2020. The Landsat program offers global coverage at 30 m spatial resolution with a nominal 16-day revisit time (reduced to 8 days when two satellites operate concurrently) (Christopherson et al., 2019; Wulder et al., 2016). We used the Google Earth Engine (GEE) platform (Gorelick et al., 2017; Zhao et al., 2021) to download the images and to retrieve (by spatial intersection) the exposure of each residential location. All Landsat images were obtained in GEE as Collection 2 Level-2 Surface Reflectance products, which include radiometric calibration, atmospheric correction, BRDF normalization, and cross-sensor harmonization across TM, ETM+, and OLI. These standardized corrections substantially reduce known spectral differences between sensors, allowing spectral indices to be compared consistently throughout the 1985-2020 period.

Additionally, we derived indices describing the extent and type of vegetation cover around each subject from CORINE Land Cover (CLC) land use maps (Bossard et al., 2000; Büttner et al., 2012) at a spatial resolution of 50 m, downloaded from the Geoportal of the Emilia-Romagna Region. For the selected provinces, land use data were available for 1994, 2003, 2008, 2014, 2017, and 2020. For intermediate years, we applied a temporal interpolation strategy. Each time interval between two consecutive maps was divided in half: the first half was attributed to the older map, and the second half to the more recent map.

To support a quantitative comparison with a land-cover dataset independent of the GEI construction, we used the Copernicus High Resolution Layer (HRL) Imperviousness dataset (Copernicus Land Monitoring Service, 2018), derived from European Union's Copernicus Land Monitoring Service information, with a spatial resolution of 20 m. This dataset provides the percentage of impervious surfaces and can be interpreted as an indirect measure of urbanized land. The data were available for the years 2006, 2009, 2012, 2015, 2018, and 2021.

Depending on the index type, we centered buffers either on the residential location (individual) or on the green space itself using the QGIS software (QGIS Development Team, 2024; Rosas-Chavoya et al., 2022).

A schematic diagram of the data sources and research workflow is provided in Fig. 1.

2.2. Green space exposure indices

We extracted NDVI (Huang et al., 2021; Ozyavuz et al., 2015; Pettorelli et al., 2005; Tucker, 1979; Xu et al., 2022) and Tasseled Cap Greenness values (Crist and Cicone, 1984; Healey et al., 2005; Kauth and Thomas, 1976). NDVI was computed in GEE using the standard formulation (NIR − Red)/(NIR + Red) applied to atmospherically corrected surface reflectance bands. Negative NDVI values (non-vegetated surfaces) were reclassified to 0 prior to all green space metric calculations to avoid interference in spatial aggregation. Tasseled Cap Greenness was derived in GEE using the sensor-specific coefficients provided for Landsat TM, ETM+, and OLI, and was computed from the same surface reflectance products to ensure temporal and radiometric consistency.

Both NDVI and Tasseled Cap Greenness were computed for circular buffers of 100 m, as recommended by previous studies (Dadvand et al., 2012a, 2012b; Donovan et al., 2011; Markevych et al., 2017; Vinceti et al., 2017a), and 200 m (see flowchart in Fig. S2). To refine the estimation, we also defined a second type of buffer, hereafter quoted as "green buffer", by clipping circular buffers to areas classified as green space in the CLC dataset (e.g., parks, forests, meadows). This approach refined the spatial aggregation by including only those pixels that fell within actual green areas. For each type of buffer, we computed both annual and seasonal (April-May-June) averages to analyze the effect of selecting different temporal windows. Cloud-free images were not available for the AMJ period in 1991, 1994, and 1999. Seasonal averages were therefore not calculated for these years, which were excluded from subsequent analyses.

Green space exposure was quantified using combinations of

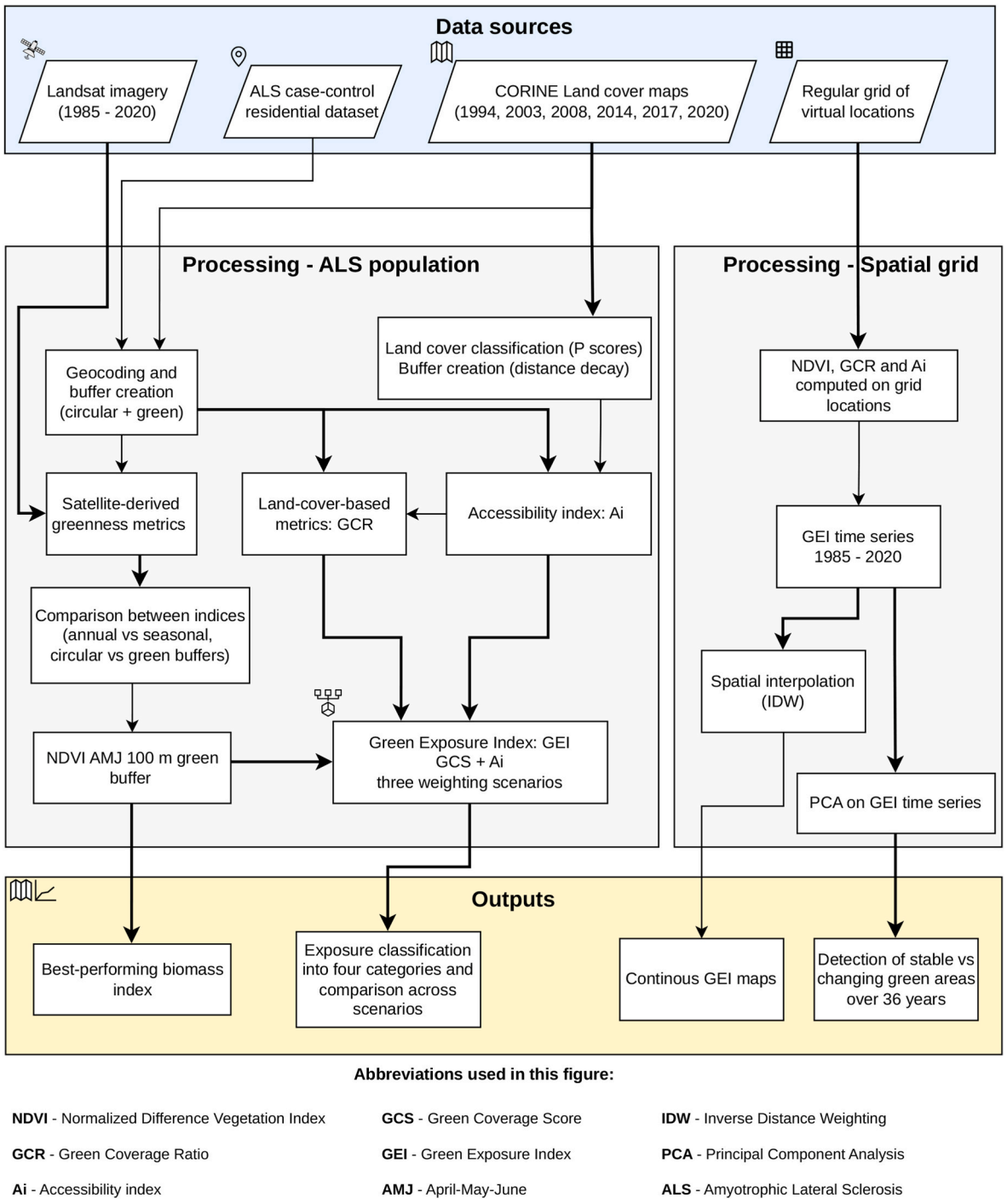

Fig. 1. Schematic diagram of the data sources and research workflow. The figure summarizes the datasets used (Landsat imagery, CORINE Land Cover and residential/grid locations) and the main analytical steps leading to the computation of the GEI, including the spatial and temporal analyses.

vegetation index (NDVI or Greenness), buffer size (100 m or 200 m), buffer type (circular or green), and temporal aggregation (annual or AMJ). Specifically, $TC(G)_{y100}$ represents the annual Greenness within a 100-m circular buffer; $NDVI_{y100}$ and $NDVI_{y200}$ correspond to the annual NDVI values within 100-m and 200-m circular buffers, respectively; $NDVI_{amj}$ refers to the April-May-June seasonal NDVI within a 100-m circular buffer; and $NDVI_{green}$ denotes the AMJ NDVI calculated within a 100-m green buffer.

A comparative analysis was conducted to assess the effect of vegetation index type, buffer size, temporal averaging, and buffer type on green space exposure estimates, in order to identify the most suitable satellite-based configuration for the GEI computation. The Pearson correlation coefficient (95% CI) quantified the relationships between indices, and differences between homogeneous indices were examined. Symmetric, near-zero differences distributions indicated comparable vegetation representation, while asymmetric distributions revealed systematic deviations.

Vegetation extent within a fixed buffer was quantified using the Green Coverage Ratio (GCR), ranging from 0 to 1 (Cao et al., 2023; Ouyang et al., 2020; Tian et al., 2011; Yuan et al., 2021):

$$GCR = \frac{A_{green}}{A_{tot}} \quad (1)$$

Where A_{green}/A_{tot} represents the fraction of vegetated area within the buffer.

To quantify green space accessibility, we developed an index Ai designed for long-term, large-scale individual exposure assessments. The index accounts for the distance between the residential location and surrounding green spaces (among a circular buffer), and the "quality" of the green spaces (urban parks, agricultural lands or forests, etc.). We grouped land use data derived from CLC maps into three categories.

- Artificial non-agricultural vegetated areas (e.g., urban parks);
- Forested and semi-natural environments;
- Agricultural territories.

We adopted a classification based on macro-categories to ensure large-scale applicability across the entire temporal domain. We assigned accessibility scores (P) to each category. These scores represent potential accessibility rather than actual observed use and are based on the degree of public access associated with different types of green spaces. Since there are no universally accepted standards for assigning accessibility scores to green spaces (Ekkel and De Vries, 2017; Semenzato et al., 2023), we adopted a scoring system that reflects differences in public access among the three categories. The assigned scores are semi-quantitative values that follow an ordinal scale, representing a numerical coding that indicates a functional hierarchy (Li et al., 2018). Artificial non-agricultural vegetated areas were used as the reference for maximum potential accessibility (P = 1), as many are explicitly designated for recreational purposes and typically have few or no access restrictions. Forested and semi-natural environments were assigned an intermediate score (P = 0.7) to reflect less immediate access conditions, since visiting these areas often requires more deliberate planning and effort than visiting urban parks. Agricultural territories were assigned the lowest accessibility score (P = 0.4) due to the limited public access typically associated with privately owned farmland, which often has access restrictions and serves a different primary function (Browning et al., 2022; Ekkel and De Vries, 2017; Pastore et al., 2026; Semenzato et al., 2023). The spacing between the assigned values was chosen to reflect substantial, but not extreme, differences in accessibility. These P-values correspond to three discrete accessibility levels (high, moderate, low) assigned to green space categories, while the continuous component of the index arises exclusively from the distance-decay function described below.

To reflect decreasing accessibility with distance, we applied the following logarithmic function:

$$Ai(d) = P\left[1 - \frac{\ln(d) - \ln(100)}{\ln(1300) - \ln(100)}\right] \quad (2)$$

Where:

Ai(d): accessibility index at distance d from the green space centroid;

P: accessibility score;

d: distance in meters from the green space centroid.

The logarithmic decay law is one of the possible approaches for describing the nonlinear variation of accessibility to a service as a function of distance (Liu et al., 2017; Shu et al., 2024; Taylor, 1971). Although alternative decay functions exist (e.g., negative power law, Gaussian, exponential), we adopted a logarithmic function as a modeling choice to represent potential accessibility to green areas. One advantage of this formulation is that it does not introduce additional parameters requiring calibration.

The function was defined as follows:

- d = 100 m, Ai = P;
- d = 1300 m, Ai = 0.

As shown in Fig. S3, Ai ranges between 0 and 1, decreasing progressively with distance. We computed a discrete Ai value every 100 m from each green space centroid. Within each interval, Ai was considered constant. The outermost band (1200-1300 m) defined the accessibility threshold: the accessibility score was set to zero within this interval. This threshold corresponds to the distance covered in approximately 15 min of walking at an average speed of 4.8 km/h (Seyfried et al., 2005; Weidmann, 1992), consistent with the "15-min city" paradigm. The choice of a reference walking speed independent of individuals' health status enhances the comparability and generalizability of results and reflects the potential-accessibility perspective of the index, which focuses on long-term environmental exposure.

Green space centroid-residence distance was preferred over edge distance because it provides smoother and more spatially consistent accessibility gradients, particularly for irregular or elongated green polygons. Moreover, edge-based distance may overestimate actual accessibility, as park boundaries often coincide with physical barriers (e.g., fences). At the same time, data on pedestrian access to green spaces were not consistently available across the study area and period and were therefore not applicable to a large-scale analysis such as the one conducted in this study.

We implemented the Ai computation in QGIS. Each green polygon received a P-score based on land use. From the centroid of each green area, a 1300-m buffer was created and divided into 13 concentric rings of 100 m each (Fig. S4). For each ring, we computed the corresponding Ai value using Equation (2). Where residential locations were within overlapping buffers from multiple green areas, we assigned the maximum score, assuming that individuals would preferentially use the green space offering the greatest accessibility. Physical barriers and pedestrian or road network structures were not incorporated because harmonized datasets were not consistently available across municipalities or across the 1985-2020 period. These aspects were considered during the index design, but a distance-based formulation was preferred to ensure spatial and temporal applicability. The accessibility component remains flexible and could incorporate network- or barrier-based information in future applications if suitable data becomes available.

2.3. The green exposure index (GEI)

We developed a composite index, the Green Exposure Index, to integrate the complementary metrics quantified in this study (vegetation density, green space coverage and accessibility):

$$GEI = w_1\sqrt{NDVI \cdot GCR} + w_2 A_i \quad (3)$$

where $w_1 + w_2 = 1$. The GEI was formulated using a weighted additive aggregation, in line with recommended methodologies for constructing composite indices (Figueira et al., 2005; Handbook on Constructing Composite Indicators, 2005; Nardo et al., 2005). The weights w_1 and w_2 represent the relative contributions of two conceptually different dimensions of exposure to green areas: green space availability around each residential location and accessibility to green areas within a 15-min walking distance, respectively. These weights represent parameters that should be adjusted based on the epidemiological hypothesis, the characteristics of the study population, and the specific context of the research.

The first term, $\sqrt{NDVI \cdot GCR}$, hereafter referred to as the Green Coverage Score (GCS), represents the combined effect of vegetation biomass and spatial extent around each residential location, two complementary dimensions of green space availability. NDVI and GCR were combined multiplicatively to reflect a relationship in which both components are necessary conditions, and the absence of either component implies negligible exposure. Because both NDVI and GCR are normalized to values below unity, their simple product would compress the GCS, reducing its relative contribution compared with accessibility in the definition of the GEI. To mitigate this effect while preserving the structure of the GCS, a square-root transformation was applied to restore scale comparability between GCS and Ai under equal weighting.

NDVI, GCR (Equation (1)), Ai (Equation (2)), and consequently GCS, are dimensionless components, oriented in the same direction, and normalized to a common scale ranging from 0 to 1. This ensures that the components are comparable and suitable for aggregation into a composite index. The GEI therefore ranges from 0 to 1, and the choice of weights represents an operational choice regarding the relative importance assigned to these two dimensions in the exposure assessment.

We classified the GEI and its components into four exposure categories: Not Exposed (NE) for values between 0 and 0.2, Mildly Exposed (ME) for values from 0.2 to 0.4, Exposed (E) for values from 0.4 to 0.6, and Highly Exposed (HE) for values between 0.6 and 1.To explore the general behavior of the GEI across the full range of possible weight values (Handbook on Constructing Composite Indicators, 2005), we computed the GEI under 11 different configurations obtained by varying w_1 from 0 to 1 with steps of 0.1 (Dogan, 2021; Więckowski and Sałabun, 2023), with $w_2 = 1 - w_1$. For each configuration, results were classified according to the four exposure categories, and the proportion of the study population falling into each category was calculated. We also examined how the proportion of individuals classified into the intermediate categories (ME + E) varied with w_1.

Since the choice of weights depends on the epidemiological hypothesis and the health outcome of interest, we defined three illustrative weighting scenarios to explore how different relative contributions of residential green space availability and accessibility influence GEI values. In the first scenario (GEI1), accessibility was prioritized ($w_1 = 0.3$, $w_2 = 0.7$) providing a perspective in which proximity to green spaces plays a predominant role. In the second (GEI2), the Green Coverage Score was prioritized ($w_1 = 0.7$, $w_2 = 0.3$) producing an exposure estimate mainly determined by the quantity and density of vegetation surrounding residential locations. In the third (GEI3), equal weights were assigned to both components ($w_1 = 0.5$, $w_2 = 0.5$) representing a balanced configuration.

The specific weight values 0.3, 0.5, and 0.7 were selected as illustrative, moderate, and symmetric reference values, consistent with scenario analysis practices in multi-criteria environmental assessment, where conceptual alternatives are commonly represented using low, medium, and high weight configurations (Figueira et al., 2005; Munda, 2004). These values are not based on a theoretical foundation or empirical calibration; rather, they ensure that each scenario corresponds to a distinct interpretation of exposure, while avoiding excessively extreme weight values that could lead to the dominance of a single component (Munda, 2004).

To complement this scenario-based exploration, we conducted a sensitivity analysis of the three illustrative scenarios to assess their local stability (Handbook on Constructing Composite Indicators, 2005). Methodological details are provided in Section S1 of the Supplementary Materials.

To characterize the spatial distribution of green exposure, we applied the GEI to a 50 m grid of virtual residential locations across Modena (a middle-sized city located within the Po Valley). Interpolated maps for each available year were generated using the Inverse Distance Weighting method (Shepard, 1968), to illustrate large-scale spatial patterns for the three scenarios GEI1, GEI2, and GEI3. This approach was used to explore how assigning different weights shapes the spatial pattern of GEI in the study area. The interpolated surfaces are intended for illustrative purposes only; all subsequent analyses were conducted using the original grid-point values.

To examine how different GEI scenarios related to an independent land-cover dataset, we analyzed the association between GEI values and HRL imperviousness at grid points using Spearman's rank correlation coefficient (95% CI) (Akoglu, 2018; Schober et al., 2018; Spearman, 1904).

As an additional application, we analyzed the GEI time series to identify spatial and temporal patterns related to urban green spaces. For each year, we calculated the spatial mean of GEI3 along with the 5th and 95th percentiles. To examine regional differences in exposure over time, we assigned each grid point to an exposure region using two indicators: GEI_{start}, defined as the mean GEI over the first five years of the study period (1985 - 1989), and GEI_{end}, defined as the mean GEI over the last five years (2016 - 2020). Five-year windows were used to reduce interannual variability. We classified GEI_{start} and GEI_{end} according to the four exposure categories used in this study and defined four regions: Stable Low, if both GEI_{start} and GEI_{end} fell within the two lowest exposure categories (NE, ME); Stable High, if both fell within the two highest categories (E, HE); Increasing, if GEI_{start} was in the two lowest categories and GEI_{end} in the two highest; and Decreasing, if GEI_{start} was in the two highest categories and GEI_{end} in the two lowest. For each region, we calculated the annual mean of GEI3 and its standard deviation across the study period. Based on the temporal trends of the annual mean GEI3 for each region, we estimated the rate of change (95% CI) and the coefficient of determination (R^2).

To assess long-term patterns, PCA was applied to the GEI3 time series (1985-2020), organized as a matrix of grid points (observations) x years (variables). The first principal component (PC1) represents the direction of maximum variance within the dataset, while subsequent components capture the remaining variability along orthogonal axes (Abdi and Williams, 2010). To facilitate the interpretation of the results, we calculated the eigenvalues and the percentage of variance explained by each component. To determine how many principal components should be retained and which might reflect random noise, we applied Horn's parallel analysis (Horn, 1965; Ledesma and Valero-Mora, 2007). For 1000 simulations, the values in the original dataset were randomly permuted within each column (i.e., within each year). PCA was then applied to each simulated dataset, and the observed eigenvalues were compared with the 95th percentile of the simulated eigenvalue distribution. To assess the stability of the loadings for the retained components, we performed bootstrap resampling of the observations with replacement (Diaconis and Efron, 1983), generating 1000 replicates. PCA was applied to each replicate, and the similarity between the bootstrap loading vectors and the original loading vectors was quantified using Tucker's congruence coefficient (Lorenzo-Seva and Ten Berge, 2006). From the distribution of Tucker's coefficients, we extracted the median, as well as the 5th and 95th percentiles. Significant deviations along the second principal component (PC2) may indicate areas (pixels) where the GEI has evolved differently over time. For these areas, we extracted the GEI time series to study its evolution over time.

3. Results

3.1. Comparisons between satellite-derived indices

Fig. 2 represents the trends of annual Pearson correlation coefficients across the study period, and Fig. S5 represents frequency distributions of the differences for each comparison for the year 2005, taken as the reference year.

NDVI and Greenness showed a strong correlation, with $r \geq 0.94$ across all years (Fig. 2a)

Correlations between exposure values computed with 100 m and 200 m buffers remained consistently high ($r = 0.94$ - 0.96, Fig. 2b). The analysis of the differences revealed a symmetric distribution centered around zero (Fig. S5a).

In contrast, annual and April-May-June (AMJ) seasonal averages were less correlated, with $r = 0.77$ - 0.99 (Fig. 2c) The distribution of the differences between annual and seasonal NDVI values showed slight asymmetry and a non-zero mean (Fig. S5b).

Finally, NDVI values derived from green buffers showed strong agreement with those from circular buffers ($r > 0.80$, Fig. 2d). This similarity was further confirmed by the distribution of differences, which was symmetric and centered around zero (Fig. S5c).

Based on the findings reported in this section, we selected $NDVI_{green}$ as the most appropriate satellite-derived index to be used in the GEI computation.

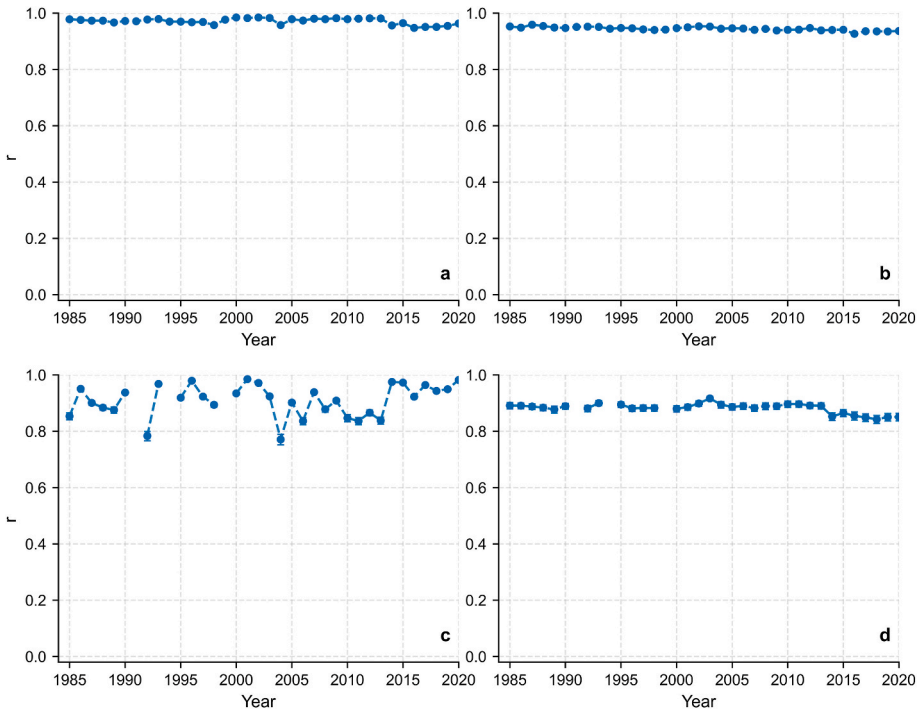

Fig. 2. Trends of yearly Pearson's correlation coefficients (r values) across the entire study period for each comparison between alternative exposure configurations: (a) NDVI vs. Greenness, (b) 100 m vs. 200 m buffers, (c) annual vs. seasonal (AMJ) NDVI, and (d) circular vs. green buffers.

3.2. Comparison of the different GEI scenarios on the case-control dataset

Table 1 reports the distribution of individuals across the four exposure categories described in Section 2.3 for the 11 weight configurations for the year 2005, taken as the reference year. As w_1 increased, the proportion of individuals classified as NE increased from 0.6% to 49.2%, with minor fluctuations at low w_1 values. Conversely, HE decreased from 43.2% to 11.7%, with small fluctuations at higher w_1 values. The intermediate categories did not show monotonic trends: ME reached its maximum value at 39.5% when $w_1 = 0.5$, while E reached its maximum value at 58.1% when $w_1 = 0.3$. Fig. 3 shows the combined proportion of individuals in ME + E. The distribution is unimodal, started at 56.2% for $w_1 = 0$, peaked at 80.1% for $w_1 = 0.4$, and decreased to 39.1% for $w_1 = 1$.

The three illustrative GEI scenarios (GEI1, GEI2, GEI3) were computed by assigning different weightings to the two components (GCS and Ai). Exposure values were classified into the four exposure categories and, for comparison, the same exposure thresholds were applied to individual indices ($NDVI_{y100}$, $NDVI_{amj}$, $NDVI_{green}$, GCR, and Ai).

Table 2 reports the percentages of residential locations in each category for each scenario in 2005, taken as the reference year.

The most pessimistic result was given by GCR, where over half of the

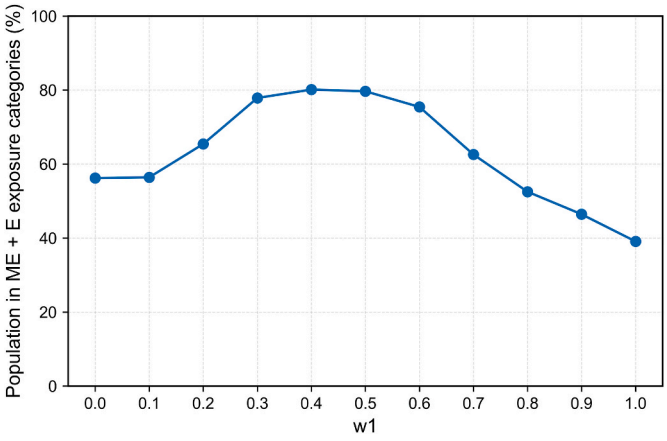

Fig. 3. Proportion of individuals classified as Mildly Exposed and Exposed across the full range of w_1.

Table 1
Distribution of individuals across the four GEI exposure categories Not Exposed, Mildly Exposed, Exposed and Highly Exposed for the 11 global weighting configurations for the year 2005, taken as the reference year.

w_1	w_2	NE	ME	E	HE
0.0	1.0	0.6%	11.3%	44.9%	43.2%
0.1	0.9	0.4%	11.9%	44.5%	43.2%
0.2	0.8	0.3%	19.6%	45.9%	34.3%
0.3	0.7	0.3%	19.7%	58.1%	21.8%
0.4	0.6	1.5%	32.6%	47.6%	18.4%
0.5	0.5	4.7%	39.5%	40.2%	15.6%
0.6	0.4	12.7%	39.2%	36.3%	11.8%
0.7	0.3	26.3%	31.9%	30.6%	11.1%
0.8	0.2	36.5%	27.0%	25.5%	11.0%
0.9	0.1	42.2%	26.8%	19.6%	11.4%
1.0	0.0	49.2%	23.4%	15.7%	11.7%

Table 2
Percentages of residential locations classified in each exposure category (NE = Not Exposed, ME = Mildly Exposed, E = Exposed, HE = Highly Exposed) for all indices and GEI scenarios in 2005, taken as the reference year.

Index	NE	ME	E	HE
$NDVI_{y100}$	3.9%	51.4%	37.1%	7.6%
$NDVI_{amj}$	2.2%	39.0%	34.9%	23.9%
$NDVI_{green}$	32.0%	19.7%	23.1%	25.3%
GCR	61.7%	18.2%	8.9%	11.2%
A_i	0.6%	13.3%	42.6%	43.5%
GEI_1	0.3%	19.7%	58.1%	21.8%
GEI_2	26.3%	31.9%	30.6%	11.1%
GEI_3	4.7%	39.5%	40.2%	15.6%

residential locations fell into the NE category, while the Ai index mainly classified them as E or HE, with almost no NE locations. GEI1 (accessibility-driven scenario) included a higher proportion of locations in the E category and substantially lower HE compared to the Ai index alone. GEI2 (green-coverage-driven scenario) reduced the proportion of NE compared to $NDVI_{green}$ alone, by integrating accessibility. Finally, GEI3 (equally weighted scenario) placed the majority of the population in the intermediate ME and E categories, while only a small proportion fell into the extreme classes.

The complete results of the sensitivity analysis for the three illustrative scenarios are available in section S1 of the Supplementary Materials.

3.3. Continuous spatial analysis and temporal dynamics of the GEI

The GEI was computed for the three scenarios on a regularly spaced grid centered on Modena. Fig. 4 shows the interpolated maps created for each scenario for 2005, taken as the reference year, with exposure values classified according to the categories defined in Section 2.3. Fig. 4a also shows the extent of the study area where the interpolated maps were generated.

In the first scenario (GEI1, Fig. 4a), where accessibility dominated, the city center included some low-exposure zones, but they were often adjacent to high-exposure areas due to the presence of nearby parks. In the second scenario (GEI2, Fig. 4b), that emphasized the contribution of vegetation around each residential location, spatial patterns generally reflected land cover: the dense urban center showed predominantly low exposure, while agricultural or natural land in the peripheral zones received higher exposure values. The third scenario provided a balanced perspective (GEI3, Fig. 4c): exposure levels better aligned with land cover with respect to the first scenario, but the contrast between exposure areas were less pronounced with respect to the second scenario, with less frequent extreme values.

The comparison between GEI values and imperviousness, conducted for 2006 as the reference year, revealed different levels of association across scenarios, with the Spearman's rank correlation coefficient increasing as greater weight was assigned to GCS. Specifically, for GEI1 the Spearman correlation coefficient was $\rho = -0.09$ (95% CI: -0.10 to -0.09), whereas for GEI3 it was $\rho = -0.40$ (95% CI: -0.40 to -0.39). For GEI2, the coefficient was $\rho = -0.55$ (95% CI: -0.56 to -0.55). The strongest association was observed when only the GCS component was considered, by assigning zero weight to the accessibility component ($\rho = -0.72$, 95% CI: -0.72 to -0.71).

The annual mean GEI3 for the entire study area did not show any clear increasing or decreasing trend and remained relatively stable over time (Fig. S6); the rate of change was 2.1×10^{-4} and not statistically significant (95% CI: -1.6×10^{-4} to 0.001), and $R^2 = 0.04$. The 5th and 95th percentiles indicated a large spatial dispersion of exposure across all years. The temporal trend of GEI3 for the four regions into which the dataset was divided are presented in Fig. S7, and their statistical characteristics are reported in Table S8. Most grid points were assigned to the stable regions, while only small fractions were classified as Increasing or Decreasing. The Increasing and Decreasing regions were characterized by a significant rate of change and high R^2 values, while the Stable High and Stable Low regions did not show significant temporal variation. Fig. S8 displays the spatial distribution of the four regions: grid points classified as Stable Low were mainly concentrated in the central and most urbanized areas of the city, while Stable High points were predominantly located in peripheral areas and within urban parks. Areas classified as Increasing or Decreasing were scattered across the map and covered only limited spatial extents.

For the GEI3 scenario, the PCA transformation was applied to the entire temporal series. The scree plot and cumulative explained variance (Fig. S9) showed that the first components accounted for most of the total variance (PC1: 81.99%; PC2: 7.11%; PC1 + PC2: 89.10%). Horn's parallel analysis indicated that only the first two components had

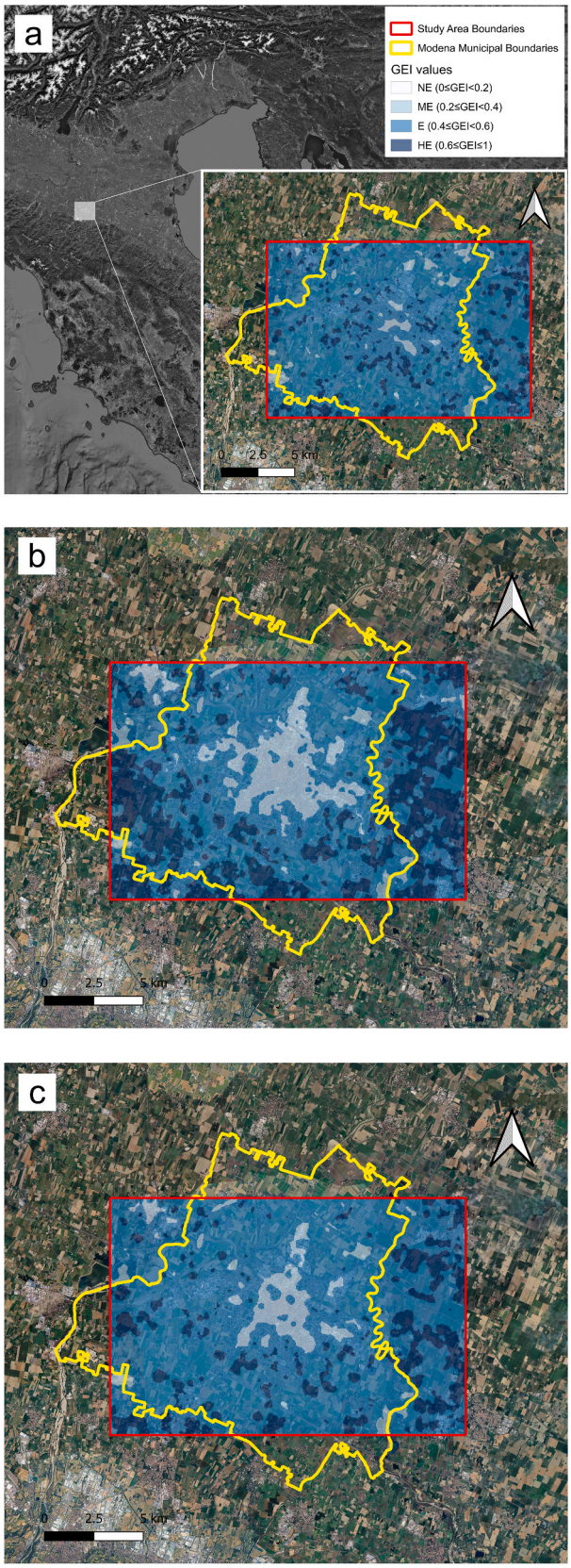

Fig. 4. Interpolated maps for: (a) the GEI1 accessibility-driven scenario, (b) the GEI2 green-coverage-driven scenario, and (c) the GEI3 equally weighted scenario, evaluated for the year 2005 in the study area around Modena, Italy.

eigenvalues larger than those expected from a random dataset; therefore, only PC1 and PC2 were retained as significant components. Tucker's congruence coefficients showed very high similarity between the original and bootstrap loading vectors for PC1 and PC2, with coefficient values greater than 0.99 in virtually all cases (>99.99%). Moreover, in 95% of the bootstrap resamples, the cumulative explained variance of PC1 and PC2 remained above 88.99%.

Fig. 5 shows the GEI scores projected along PC1. Areas with positive PC1 values largely corresponded to green spaces, while negative scores were concentrated in more urbanized zones. The projections of the GEI values along PC2 are shown in Fig. 6. PC2 represented additional variability not captured by PC1. We selected ten points of interest (Fig. 6) with high absolute PC2 scores for a detailed analysis. The temporal evolution of the GEI at these locations is shown in Fig. 7. Two main trends were observed: in areas with positive PC2 scores (e.g., A1) GEI values decreased over time; by contrast, in areas with negative PC2 scores (e.g., A3), an increase in GEI values was observed.

4. Discussion

The high correlation observed between NDVI and Tasseled Cap Greenness indicated that both indices captured highly similar information from visible and near infrared spectral bands, as expected. NDVI was retained for subsequent analyses due to its simpler formulation and broader use in the literature (Dadvand et al., 2012a, 2012b; Donovan et al., 2011; Markevych et al., 2017; Vinceti et al., 2017a). Correlations between 100 m and 200 m buffers were also consistently high. The results achieved supported the use of the 100 m buffer for computational efficiency and existing literature (Dadvand et al., 2012a, 2012b; Donovan et al., 2011; Markevych et al., 2017; Vinceti et al., 2017a). In contrast, the correlations between annual and AMJ NDVI were lower, largely due to the pronounced phenological variability of the vegetation stage within the year. To ensure a more accurate representation of actual vegetation conditions, the seasonal NDVI (AMJ) was selected for use in subsequent analyses. This choice enhances spatial discrimination by capturing vegetation during its peak growth phase and improves inter-annual differentiation. It also avoids the flattening effect associated with full-year averaging, which may mask relevant temporal dynamics and fluctuations. NDVI values derived from green and circular buffers showed strong agreement. NDVI values calculated using green buffers were selected for continued use, as this approach explicitly limits the aggregation to pixels classified as green areas and reduces the risk of overestimation of green space that can occur with circular buffers, where non-vegetated surfaces (e.g., impervious urban areas) can contribute to the index.

Exploratory analysis of the GEI's variation across the full range of possible weight values provided a useful diagnostic tool for understanding how the index responds to different assumptions about the relative importance of its two components. Rather than identifying an optimal configuration, this analysis showed that the GEI responds in a regular and predictable manner as the weights vary. This information can support future studies in selecting appropriate weights, while acknowledging that their selection must ultimately be guided by the epidemiological hypothesis and the exposure pathways relevant to the specific health outcome under investigation.

The comparison of GEI scenarios on the case-control dataset showed that residential locations varied substantially among the four exposure categories. Reducing the proportion of residential locations assigned to extreme exposure classes (as observed for GEI3) is particularly relevant in epidemiological applications, where locations are often clustered in densely urbanized areas. In this type of setting, a higher number of locations in intermediate classes provides a more realistic representation of exposure patterns, improving the sensitivity of the index and allowing the detection of subtle spatial differences in green space exposure.

The results of the sensitivity analysis of the three illustrative scenarios showed that GEI1, GEI2, and GEI3 used in this study are locally stable, with small variations in the weights producing only limited and mostly adjacent reclassifications. Together, the analyses conducted across the full range of weight values and around the three illustrative configurations supported the methodological robustness of the GEI as a flexible and adaptable index.

The spatial maps generated for the three GEI scenarios produced distinct spatial patterns that reflected the relative influence of green coverage and accessibility. GEI1 emphasized accessibility, leading to higher exposure values near public parks, historic villas and sports facilities, all included in the “Artificial, non-agricultural vegetated areas”, which were assigned the maximum accessibility score. GEI2, which assigned greater weight to vegetation cover, highlighted disparities between densely built urban centers and greener suburban peripheries. By integrating accessibility with the type of green area and biomass density, the third scenario combined the strengths of the first two scenarios: it did not underestimate low-exposure locations, and it provided additional information beyond what was captured by land use maps alone, by accounting for multiple factors that influence green space exposure. The differences observed in these patterns primarily reflected the weighting schemes, while fine-scale variations may also be influenced by the visualization method (IDW interpolation).

Comparison of the GEI scenarios with an independent land-cover

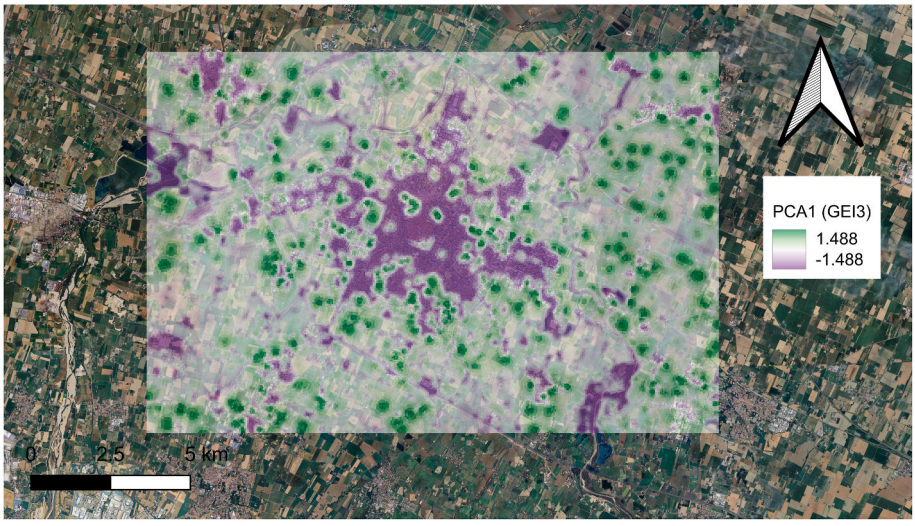

Fig. 5. PC1 score map for GEI. The false-color representation used the 95th and 5th percentiles as the maximum and minimum values, respectively.

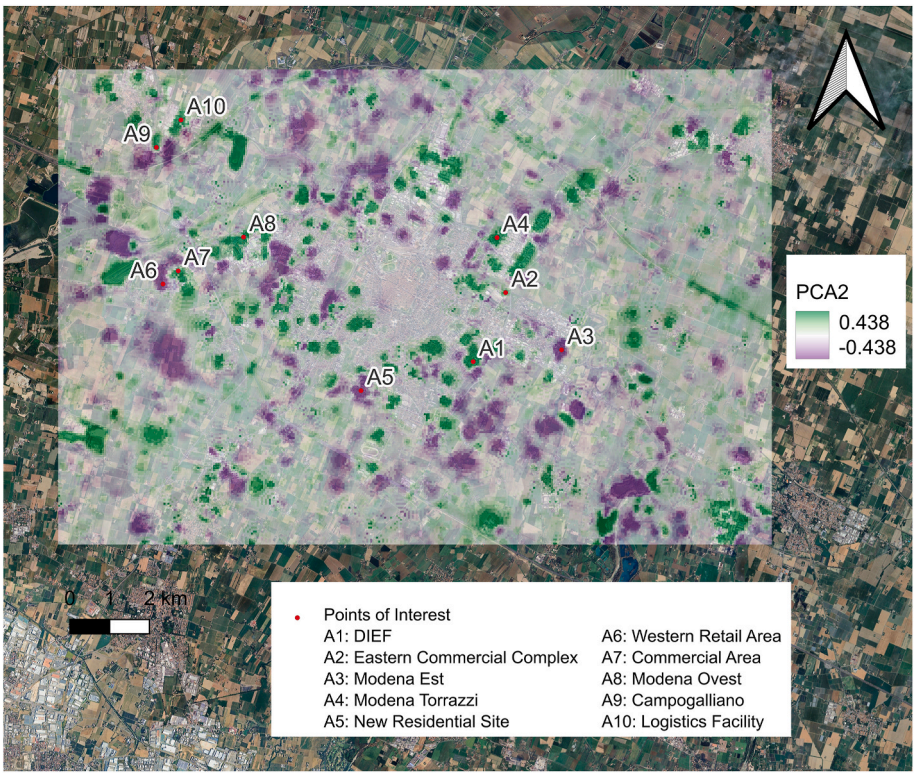

Fig. 6. Map of GEI values projected along the PC2 axis, with 10 points of interest located in areas showing high absolute PC2 scores. The false-color representation used the 95th and 5th percentiles as the maximum and minimum values, respectively.

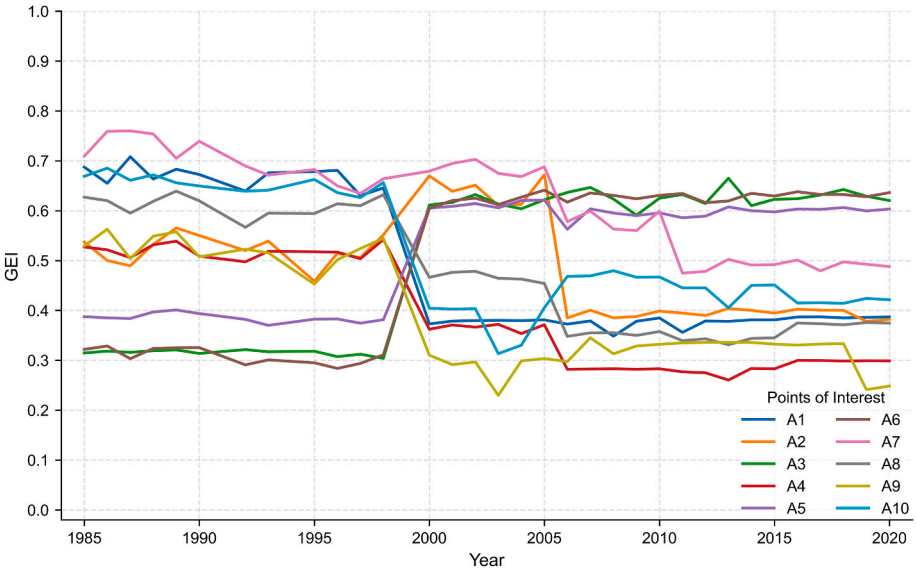

Fig. 7. Trends of the GEI values in correspondence of the 10 points of interest.

dataset, such as HRL imperviousness, revealed a negative relationship between GEI values and the fraction of impervious surface, consistent with the vegetation component of the index, while the inclusion of accessibility attenuated this relationship. This result reflected the composite nature of the GEI, which also integrates information on accessibility and therefore cannot be directly attributed to land-cover characteristics alone. Indeed, the GEI was not designed to describe or classify land-use types, but rather to integrate multiple dimensions of exposure into a single metric.

Analysis of the GEI3 time series indicated that overall exposure to green spaces in Modena remained relatively stable during the period 1985-2020, although substantial spatial differences were observed. The four exposure regions into which the dataset was classified exhibited distinct temporal trajectories, confirming the heterogeneity of the study area. The spatial distribution of grid points classified as Stable High and Stable Low aligns closely with the urban fabric of the study area, while the spatial distribution of regions classified as Increasing or Decreasing appeared to reflect local and limited changes in green space exposure.

Statistical analyses performed on the PCA results (scree plot, explained variance, parallel analysis, and bootstrap resampling) were

useful for quantitatively determining how many components to retain and for assessing their stability, thereby reducing the risk of over-interpreting their meaning. These results supported the interpretation of PC1 and PC2 as stable principal components rather than random noise, whereas the remaining components appeared to be dominated by noise. Since PC1 captured the dominant information common to the entire time series, it likely reflected long-term stable patterns. This interpretation is consistent with well-known characteristics of the study area: the areas identified by PC1, such as the city center or the main urban parks, remained relatively unchanged over the study period. Since PC2 captured the residual variability in the dataset, areas associated with extreme PC2 values might have followed distinct temporal evolutions with respect to the dominant pattern captured by PC1. The analysis of the ten points of interest with extreme PC2 scores showed that these locations experienced changes in green exposure over the study period. Changes can be linked to land use change, as in the A1 site, a university area where a decline is visible in the late 1990s due to the construction of the Department of Engineering "Enzo Ferrari". In other cases, changes are not related to green expansion or consumption but to a reclassification in the land use database, as in the A3 site, a residential district in the eastern part of Modena, where an urban park present since 1985 was included in the land use database only in more recent updates.

PCA was used as an exploratory tool to summarize the GEI time series and to facilitate interpretation of the spatiotemporal dynamics of the GEI across the study area. Overall, PCA identified patterns consistent with known characteristics of the study area. These results are descriptive and exploratory in nature, but they allowed us to synthesize the annual GEI maps for the entire study period into few components that capture the dominant structure of the dataset and its main deviations.

The three scenarios defined as GEI1, GEI2, and GEI3 were used as illustrative examples to examine how different emphases on accessibility and green coverage influence GEI values. Assigning greater weight to accessibility may be appropriate for applications in which proximity to green areas is assumed to have greater epidemiological relevance than the quantity of vegetated biomass around the residential location, a perspective aligned with exposure estimates based on walkability, access, and use of green areas (Giles-Corti et al., 2005; Twohig-Bennett and Jones, 2018). Conversely, assigning greater weight to local vegetation density and extent is consistent with assessments that emphasize the health benefits of green areas (e.g., improved air quality, mitigation of the urban heat island effect) (Bowler et al., 2010; Nowak et al., 2014). A balanced weight configuration can provide a neutral starting point for exploratory analyses in epidemiological applications when there is no clear rationale for privileging one aspect over the other. In all cases, the choice of weights should be tailored to the epidemiological hypothesis and the specific context of the study.

The GEI was developed within a specific European context, but its structure was designed to be transferable to other geographical areas. The use of a weighted-sum formulation with adjustable weights allows for substantial adaptability depending on the epidemiological hypothesis and local context. The use of normalized, dimensionless components also facilitates interpretation and comparability of the index across regions. The satellite-derived vegetation component (NDVI) is globally available. When the CLC dataset is not available (e.g., outside Europe), the GCR can be derived from alternative land-cover products such as the ESA WorldCover dataset (Zanaga et al., 2021), although these alternatives do not currently offer time series as extensive as CLC. The accessibility component can be adapted to the green-space governance and mobility characteristics of the study area. The accessibility scores P reflect levels of public access typical of the European context, and should be adjusted when accessibility conditions differ. In the absence of continuous pedestrian-network data, or for large-scale applications, Euclidean distance still allows the index to be applied. The accessibility threshold can be modified to reflect mobility patterns that differ from those of compact European cities, such as those in car-dependent contexts. Ultimately, the accuracy of the GEI depends on the resolution of the land cover dataset used and on the availability of pedestrian-network data, and is therefore linked to the context and scale of the study.

Regarding study limitations, we acknowledge that the land cover component relied on irregularly updated datasets, with land use assumed to remain unchanged between the reference years. The stepwise temporal interpolation we adopted can advance or delay land-use changes, particularly affecting indices derived directly from the land-cover dataset, such as GCR and Ai. The error introduced by these assumptions becomes more pronounced in areas undergoing rapid urban transformation and in earlier decades, when CLC updates were less frequent. As a result, the GEI time series exhibited a stepwise pattern, as shown in Fig. 7 and S7, with steps reflecting the transition between successive land-cover datasets. These discontinuities do not invalidate regional trends but influence their shape, which would otherwise appear smoother and more continuous. Moreover, any inaccuracies or inconsistencies in land use maps directly affect quantification, particularly compromising temporal analyses. This effect is especially evident in the analysis of point of interest A3 (Fig. 7), where an apparent increase in exposure was observed despite no actual expansion of green areas.

Concerning satellite imagery limitations in computing NDVI and TCG indices, limited availability of suitable cloud-free images in the AMJ period resulted in the exclusion of three years (1991, 1994, and 1999) from the analysis, slightly reducing temporal coverage.

Finally, we assessed pedestrian accessibility using a circular buffer representing a 15-min walking distance from each residential location, calculated as a straight-line distance. This method does not reflect the actual structure of the road network and fails to account for physical barriers such as rivers, railways, or other infrastructures that cannot be crossed on foot. The use of Euclidean distance can lead to an overestimation of accessibility in dense urban settings. This error is not uniform but spatially structured, as it depends on urban morphology and the presence of physical barriers (Droin et al., 2024; Yenisetty and Bahadure, 2020). As a result, the precision of accessibility estimates at specific locations may be reduced, and individuals who fall just below the accessibility threshold may not, in practice, have access to a green space within a 15-min walk.

Even with these constraints, we believe that the GEI we presented could offer a more comprehensive and flexible framework to assess green space exposure in epidemiologic studies and other contexts like urban planning. By accounting for both environmental features and accessibility, the index aligns more closely with real-world exposure dynamics and significance. Furthermore, the possibility to modulate the weights of its components allows for tailored applications: for example, in populations with limited mobility (e.g., the elderly or disabled), the local vegetation component may be more relevant, while for general urban planning, walkable access to public green space is a key determinant of exposure (James et al., 2015).

5. Conclusions

This study developed and tested a composite Green Exposure Index that integrates vegetation biomass, land cover, and accessibility to capture multiple dimensions of green space exposure. After the comparisons between satellite-derived indices, the NDVI (AMJ) configuration with 100 m green buffer was identified as the most suitable vegetation proxy among the options tested in this study and was adopted for GEI computation. The three weighting scenarios (GEI1, GEI2, GEI3) demonstrated the tool's flexibility in adapting to different epidemiological or urban contexts. The green space exposure indices compared and selected in this study will be applied to other datasets currently under investigation. The exposure estimates from both this and the other datasets will be used to conduct statistical analyses aimed at exploring potential associations between long-term exposure to green spaces and the onset of neurodegenerative diseases. The GEI will be further tuned as

needed according to the specific application, context, and study population.

Beyond health studies, the GEI offers a flexible framework for urban and environmental planning, supporting the assessment of how green space interventions affect population-level exposure.

Future developments of the GEI may include integrating metrics based on actual pedestrian networks to provide more accurate estimates of accessibility, while also combining the GEI with other environmental factors related to mental health (such as air pollution, urban heat island effects, and exposure to artificial light at night). Finally, incorporating sociodemographic and behavioral data could enhance the interpretation of exposure to greenery and improve predictive capacity in complex epidemiological contexts.

CRediT authorship contribution statement

Niccolò Martini: Writing – review & editing, Writing – original draft, Visualization, Software, Methodology, Investigation, Formal analysis, Data curation, Conceptualization. **Francesca Despini:** Writing – review & editing, Supervision, Software, Methodology, Investigation, Formal analysis, Data curation, Conceptualization. **Tommaso Filippini:** Writing – review & editing, Supervision, Resources, Project administration, Investigation, Formal analysis, Data curation, Conceptualization. **Marco Vinceti:** Writing – review & editing, Supervision, Resources, Project administration, Methodology, Investigation, Conceptualization. **Sergio Teggi:** Writing – review & editing, Supervision, Project administration, Methodology, Conceptualization. **Sofia Costanzini:** Writing – review & editing, Validation, Supervision, Software, Project administration, Methodology, Investigation, Formal analysis, Data curation, Conceptualization.

Funding

This study was supported by grant “PRIN 2022” (no. 2022MHMRPR) from the Italian Ministry of University and Research (MUR) funded by European Union—Next Generation EU, and by grant “UNIMORE FAR 2023” from the University of Modena and Reggio Emilia. Tommaso Filippini was also supported by grant "PRIN 2022 PNRR” (no. P20229KSXB) from the Italian Ministry of University and Research (MUR) funded by European Union—Next Generation EU. The funders had no role in the design and conduct of the study, collection, management, analysis, interpretation of the data, preparation, review, approval, nor decision to submit the manuscript for publication.

Declaration of competing interest

The authors declare that they have no known competing financial interests or personal relationships that could have appeared to influence the work reported in this paper.

Appendix A. Supplementary data

Supplementary data to this article can be found online at https://doi.org/10.1016/j.envres.2026.124254.

Data availability

Data will be made available on request.

References

Abdi, H., Williams, L.J., 2010. Principal component analysis. WIREs Computational Stats 2, 433–459. https://doi.org/10.1002/wics.101.

Akoglu, H., 2018. User's guide to correlation coefficients. Turkish Journal of Emergency Medicine 18, 91–93. https://doi.org/10.1016/j.tjem.2018.08.001.

Ashinze, U.K., Edeigba, Blessing Aibhamen, Umoh, Aniekan Akpan, Biu, Preye Winston, Daraojimba, Andrew Ifesinachi, 2024. Urban green infrastructure and its role in sustainable cities: a comprehensive review. World J. Adv. Res. Rev. 21, 928–936. https://doi.org/10.30574/wjarr.2024.21.2.0519.

Bagheri, N., Mavoa, S., Tabatabaei-Jafari, H., Knibbs, L.D., Coffee, N.T., Salvador-Carulla, L., Anstey, K.J., 2021. The impact of built and social environmental characteristics on diagnosed and estimated future risk of dementia. J. Alzheimers Dis. 84, 621–632. https://doi.org/10.3233/JAD-210208.

Bannari, A., Morin, D., Bonn, F., Huete, A.R., 1995. A review of vegetation indices. Remote Sens. Rev. 13, 95–120. https://doi.org/10.1080/02757259509532298.

Barbosa, O., Tratalos, J.A., Armsworth, P.R., Davies, R.G., Fuller, R.A., Johnson, P., Gaston, K.J., 2007. Who benefits from access to green space? A case study from Sheffield, UK. Landsc. Urban Plann. 83, 187–195. https://doi.org/10.1016/j.landurbplan.2007.04.004.

Bossard, M., Feranec, Ján, Otahel, Jan, 2000. CORINE Land Cover Technical Guide – Addendum 2000 (Technical Report No. 40). European Environment Agency, Copenhagen.

Bowler, D.E., Buyung-Ali, L., Knight, T.M., Pullin, A.S., 2010. Urban greening to cool towns and cities: a systematic review of the empirical evidence. Landsc. Urban Plann. 97, 147–155. https://doi.org/10.1016/j.landurbplan.2010.05.006.

Browning, M.H.E.M., Rigolon, A., Ogletree, S., Wang, R., Klompmaker, J.O., Bailey, C., Gagnon, R., James, P., 2022. The PAD-US-AR dataset: measuring accessible and recreational parks in the contiguous United States. Sci. Data 9, 773. https://doi.org/10.1038/s41597-022-01857-7.

Büttner, G., Kosztra, B., Maucha, G., Pataki, R., 2012. Implementation and Achievements of CLC2006. European Environment Agency (EEA), Copenhagen. https://doi.org/10.2909/71c95a07-e296-44fc-b22b-415f42acfdf0.

Cao, Y., Li, G., Huang, Y., 2023. Spatiotemporal evolution of residential exposure to green space in Beijing. Remote Sens. 15, 1549. https://doi.org/10.3390/rs15061549.

Christopherson, J.B., Ramaseri Chandra, S.N., Quanbeck, J.Q., 2019. 2019 Joint Agency Commercial Imagery Evaluation - Land remote sensing satellite compendium (Circular), 1455. U.S. Geological Survey. https://doi.org/10.3133/cir1455.

Clark, C.J., Haynes, D., Lu, Z., Sample, J.M., McGuinn, L.A., Hoang, T.T., Lupo, P.J., Scheurer, M.E., Marcotte, E.L., Williams, L.A., 2025. Ambient fine particulate matter, residential greenness, and childhood cancer risk by trimester of exposure in Minnesota 2000 to 2014: a case–control Study. Cancer Epidemiol. Biomarkers Prev. 34, 1730–1739. https://doi.org/10.1158/1055-9965.EPI-25-0465.

Copernicus Land Monitoring Service, 2018. Copernicus High Resolution Layer Imperviousness. https://doi.org/10.2909/532f0b73-66c3-46f6-b5a5-d1cccd140433.

Costanzini, S., Boccolari, M., Vega Parra, S., Despini, F., Lombroso, L., Teggi, S., 2024. A comparative analysis of temperature trends at Modena geophysical observatory and mount cimone observatory, Italy. Intl Journal of Climatology 44, 4741–4766. https://doi.org/10.1002/joc.8607.

Costanzini, S., Teggi, S., Bigi, A., Ghermandi, G., Filippini, T., Malagoli, C., Nannini, R., Vinceti, M., 2018. Atmospheric dispersion modelling and spatial analysis to evaluate population exposure to pesticides from farming processes. Atmosphere 9, 38. https://doi.org/10.3390/atmos9020038.

Crist, E.P., Cicone, R.C., 1984. A physically-based transformation of thematic mapper data-the TM tasseled cap. IEEE Trans. Geosci. Rem. Sens. 22, 256–263. https://doi.org/10.1109/TGRS.1984.350619.

Dadvand, P., De Nazelle, A., Figueras, F., Basagaña, X., Su, J., Amoly, E., Jerrett, M., Vrijheid, M., Sunyer, J., Nieuwenhuijsen, M.J., 2012a. Green space, health inequality and pregnancy. Environ. Int. 40, 110–115. https://doi.org/10.1016/j.envint.2011.07.004.

Dadvand, P., Sunyer, J., Basagaña, X., Ballester, F., Lertxundi, A., Fernández-Somoano, A., Estarlich, M., García-Esteban, R., Mendez, M.A., Nieuwenhuijsen, M.J., 2012b. Surrounding greenness and pregnancy outcomes in four Spanish birth cohorts. Environ. Health Perspect. 120, 1481–1487. https://doi.org/10.1289/ehp.1205244.

Dadvand, P., Villanueva, C.M., Font-Ribera, L., Martinez, D., Basagaña, X., Belmonte, J., Vrijheid, M., Gražulevičienė, R., Kogevinas, M., Nieuwenhuijsen, M.J., 2014. Risks and benefits of green spaces for children: a cross-sectional study of associations with sedentary behavior, obesity, asthma, and allergy. Environ. Health Perspect. 122, 1329–1335. https://doi.org/10.1289/ehp.1308038.

Diaconis, P., Efron, B., 1983. Computer-intensive methods in statistics. Sci. Am., 248, 116-131.

Dogan, O., 2021. Process mining technology selection with spherical fuzzy AHP and sensitivity analysis. Expert Syst. Appl. 178, 114999. https://doi.org/10.1016/j.eswa.2021.114999.

Donovan, G.H., Michael, Y.L., Butry, D.T., Sullivan, A.D., Chase, J.M., 2011. Urban trees and the risk of poor birth outcomes. Health Place 17, 390–393. https://doi.org/10.1016/j.healthplace.2010.11.004.

Droin, A., Wurm, M., Weigand, M., Gawlas, C., Köberl, M., Taubenböck, H., 2024. How does pedestrian permeability vary in and across cities? A fine-grained assessment for all large cities in Germany. Comput. Environ. Urban Syst. 110, 102115. https://doi.org/10.1016/j.compenvurbsys.2024.102115.

Ekkel, E.D., De Vries, S., 2017. Nearby green space and human health: evaluating accessibility metrics. Landsc. Urban Plann. 157, 214–220. https://doi.org/10.1016/j.landurbplan.2016.06.008.

European Environment Agency (EEA), 2023. Europe’s Air Quality Status 2023. European Environment Agency. doi:10.2800/59526.

European Topic Centre on Human Health and the Environment (ETC-HE), 2024. Status Report of Air Quality in Europe for Year 2023, Using Validated and up-to-date Data (ETC-HE Report 2024/5). European Environment Agency.

Figueira, J., Greco, S., Ehrogott, M., 2005. Multiple criteria decision analysis: state of the art surveys. In: International Series in Operations Research & Management Science. Springer, New York, New York, NY. https://doi.org/10.1007/b100605.
Fiore, M., Parisio, R., Filippini, T., Mantione, V., Platania, A., Odone, A., Signorelli, C., Pietrini, V., Mandrioli, J., Teggi, S., Costanzini, S., Antonio, C., Zuccarello, P., Oliveri Conti, G., Nicoletti, A., Zappia, M., Vinceti, M., Ferrante, M., 2020. Living near waterbodies as a proxy of Cyanobacteria exposure and risk of amyotrophic lateral sclerosis: a population based case-control study. Environ. Res. 186, 109530. https://doi.org/10.1016/j.envres.2020.109530.
Fong, K.C., Hart, J.E., James, P., 2018. A review of epidemiologic studies on greenness and health: updated literature through 2017. Curr. Environ. Health Rep. 5, 77–87. https://doi.org/10.1007/s40572-018-0179-y.
Gascon, M., Triguero-Mas, M., Martínez, D., Dadvand, P., Rojas-Rueda, D., Plasència, A., Nieuwenhuijsen, M.J., 2016. Residential green spaces and mortality: a systematic review. Environ. Int. 86, 60–67. https://doi.org/10.1016/j.envint.2015.10.013.
Giles-Corti, B., Timperio, A., Bull, F., Pikora, T., 2005. Understanding physical activity environmental correlates: increased specificity for ecological models. Exerc. Sport Sci. Rev. 33, 175–181. https://doi.org/10.1097/00003677-200510000-00005.
Gorelick, N., Hancher, M., Dixon, M., Ilyushchenko, S., Thau, D., Moore, R., 2017. Google Earth Engine: planetary-scale geospatial analysis for everyone. Rem. Sens. Environ. 202, 18–27. https://doi.org/10.1016/j.rse.2017.06.031.
Handbook on Constructing Composite Indicators, 2005. Methodology and user guide (OECD Statistics Working Papers No. 2005/03). OECD Statistics Working Papers. https://doi.org/10.1787/533411815016.
Healey, S., Cohen, W., Zhiqiang, Y., Krankina, O., 2005. Comparison of Tasseled Cap-based landsat data structures for use in forest disturbance detection. Rem. Sens. Environ. 97, 301–310. https://doi.org/10.1016/j.rse.2005.05.009.
Horn, J.L., 1965. A rationale and test for the number of factors in factor analysis. Psychometrika 30, 179–185. https://doi.org/10.1007/BF02289447.
Hotelling, H., 1933. Analysis of a complex of statistical variables into principal components. J. Educ. Psychol. 24, 417–441. https://doi.org/10.1037/h0071325.
Huang, S., Tang, L., Hupy, J.P., Wang, Y., Shao, G., 2021. A commentary review on the use of normalized difference vegetation index (NDVI) in the era of popular remote sensing. J. For. Res. 32, 1–6. https://doi.org/10.1007/s11676-020-01155-1.
James, P., Banay, R.F., Hart, J.E., Laden, F., 2015. A review of the health benefits of greenness. Curr. Epidemiol. Rep. 2, 131–142. https://doi.org/10.1007/s40471-015-0043-7.
Jolliffe, I.T., Cadima, J., 2016. Principal component analysis: a review and recent developments. Phil. Trans. R. Soc. A. 374, 20150202. https://doi.org/10.1098/rsta.2015.0202.
Jones, A., Ali, M.U., Mayhew, A., Aryal, K., Correia, R.H., Dash, D., Manis, D.R., Rehman, A., O'Connell, M.E., Taler, V., Costa, A.P., Hogan, D.B., Wolfson, C., Raina, P., Griffith, L., 2025. Environmental risk factors for all-cause dementia, Alzheimer's disease dementia, vascular dementia, and mild cognitive impairment: an umbrella review and meta-analysis. Environ. Res. 270, 121007. https://doi.org/10.1016/j.envres.2025.121007.
Kabisch, N., Haase, D., 2014. Green justice or just green? Provision of urban green spaces in Berlin, Germany. Landsc. Urban Plann. 122, 129–139. https://doi.org/10.1016/j.landurbplan.2013.11.016.
Kauth, R.J., Thomas, G.S., 1976. The tasselled cap – A graphic description of the spectral-temporal development of agricultural crops as seen by LANDSAT. In: Presented at the Symposium on Machine Processing of Remotely Sensed Data. Purdue University (LARS), West Lafayette, IN, USA, pp. 4B41–4B51.
Kruize, H., Van Der Vliet, N., Staatsen, B., Bell, R., Chiabai, A., Muiños, G., Higgins, S., Quiroga, S., Martinez-Juarez, P., Aberg Yngwe, M., Tsichlas, F., Karnaki, P., Lima, M. L., García De Jalón, S., Khan, M., Morris, G., Stegeman, I., 2019. Urban green space: creating a triple win for environmental sustainability, health, and health equity through behavior change. IJERPH 16, 4403. https://doi.org/10.3390/ijerph16224403.
Kwan, M.-P., Weber, J., 2003. Individual accessibility revisited: implications for geographical analysis in the twenty-first century. Geogr. Anal. 35, 341–353. https://doi.org/10.1353/geo.2003.0015.
Kwon, D., Paul, K.C., O'Sharkey, K., Paik, S.-A., Yu, Y., Bronstein, J.M., Ritz, B., 2025. Challenges in studying air pollution to neurodegenerative diseases. Environ. Res. 278, 121597. https://doi.org/10.1016/j.envres.2025.121597.
Labib, S.M., Lindley, S., Huck, J.J., 2020. Spatial dimensions of the influence of urban green-blue spaces on human health: a systematic review. Environ. Res. 180, 108869. https://doi.org/10.1016/j.envres.2019.108869.
Ledesma, R.D., Valero-Mora, P., 2007. Determining the number of factors to retain in EFA: an easy-to- use computer program for carrying out parallel analysis. Practical Assess. Res. Eval. 12, 1–11. https://doi.org/10.1037/a0025697.
Li, Z., Fan, Z., Shen, S., 2018. Urban green space suitability evaluation based on the AHP-CV combined weight method: a case study of fuping county, China. Sustainability 10, 2656. https://doi.org/10.3390/su10082656.
Liu, W., Chen, W., Dong, C., 2017. Spatial decay of recreational services of urban parks: characteristics and influencing factors. Urban For. Urban Green. 25, 130–138. https://doi.org/10.1016/j.ufug.2017.05.004.
Lorenzo-Seva, U., Ten Berge, J.M.F., 2006. Tucker's congruence coefficient as a meaningful index of factor similarity. Methodology 2, 57–64. https://doi.org/10.1027/1614-2241.2.2.57.
Markevych, I., Schoierer, J., Hartig, T., Chudnovsky, A., Hystad, P., Dzhambov, A.M., De Vries, S., Triguero-Mas, M., Brauer, M., Nieuwenhuijsen, M.J., Lupp, G., Richardson, E.A., Astell-Burt, T., Dimitrova, D., Feng, X., Sadeh, M., Standl, M., Heinrich, J., Fuertes, E., 2017. Exploring pathways linking greenspace to health: theoretical and methodological guidance. Environ. Res. 158, 301–317. https://doi.org/10.1016/j.envres.2017.06.028.
Moreno, C., Allam, Z., Chabaud, D., Gall, C., Pratlong, F., 2021. Introducing the "15-Minute city": sustainability, resilience and place identity in future post-pandemic cities. Smart Cities 4, 93–111. https://doi.org/10.3390/smartcities4010006.
Munda, G., 2004. Social multi-criteria evaluation: methodological foundations and operational consequences. Eur. J. Oper. Res. 158, 662–677. https://doi.org/10.1016/S0377-2217(03)00369-2.
Nardo, M., Saisana, M., Saltelli, A., Tarantola, S., 2005. Tools for composite indicators building (No. EUR 21682 EN). European Commission. Joint Research Centre, Ispra, Italy.
Newton, J.D., Ellis, T., Ruther, M., Boone, S.D., Baumgartner, R., Iyer, H.S., DuPré, N., 2026. The association between residential natural vegetation exposure at diagnosis and colorectal cancer-specific mortality among colorectal cancer cases in Kentucky. Environ. Res. 291, 123574. https://doi.org/10.1016/j.envres.2025.123574.
Nowak, D.J., Hirabayashi, S., Bodine, A., Greenfield, E., 2014. Tree and forest effects on air quality and human health in the United States. Environ. Pollut. 193, 119–129. https://doi.org/10.1016/j.envpol.2014.05.028.
Ouyang, W., Morakinyo, T.E., Ren, C., Ng, E., 2020. The cooling efficiency of variable greenery coverage ratios in different urban densities: a study in a subtropical climate. Build. Environ. 174, 106772. https://doi.org/10.1016/j.buildenv.2020.106772.
Ozyavuz, M., Bilgili, B.C., Salici, A., 2015. Determination of vegetation changes with NDVI method. J. Environ. Prot. Ecol. 16, 264–273.
Pastore, M.C., Parenti, C.I.M., Patetta, C., 2026. Defining publicly accessible urban green spaces for psychophysical wellbeing in the Milan metropolitan area. Cities 168, 106415. https://doi.org/10.1016/j.cities.2025.106415.
Pettorelli, N., Vik, J.O., Mysterud, A., Gaillard, J.-M., Tucker, C.J., Stenseth, N.Chr, 2005. Using the satellite-derived NDVI to assess ecological responses to environmental change. Trends Ecol. Evol. 20, 503–510. https://doi.org/10.1016/j.tree.2005.05.011.
QGIS Development Team, 2024. QGIS Geographic Information System.
Rosas-Chavoya, M., Gallardo-Salazar, J.L., López-Serrano, P.M., Alcántara-Concepción, P.C., León-Miranda, A.K., 2022. QGIS a constantly growing free and open-source geospatial software contributing to scientific development. CIG 48, 197–213. https://doi.org/10.18172/cig.5143.
Roy, D.P., Wulder, M.A., Loveland, T.R., W, C.E., Allen, R.G., Anderson, M.C., Helder, D., Irons, J.R., Johnson, D.M., Kennedy, R., Scambos, T.A., Schaaf, C.B., Schott, J.R., Sheng, Y., Vermote, E.F., Belward, A.S., Bindschadler, R., Cohen, W.B., Gao, F., Hipple, J.D., Hostert, P., Huntington, J., Justice, C.O., Kilic, A., Kovalskyy, V., Lee, Z. P., Lymburner, L., Masek, J.G., McCorkel, J., Shuai, Y., Trezza, R., Vogelmann, J., Wynne, R.H., Zhu, Z., 2014. Landsat-8: science and product vision for terrestrial global change research. Rem. Sens. Environ. 145, 154–172. https://doi.org/10.1016/j.rse.2014.02.001.
Schober, P., Boer, C., Schwarte, L.A., 2018. Correlation coefficients: appropriate use and interpretation. Anesth. Analg. 126, 1763–1768. https://doi.org/10.1213/ANE.0000000000002864.
Semenzato, P., Costa, A., Campagnaro, T., 2023. Accessibility to urban parks: comparing GIS based measures in the city of Padova (italy). Urban For. Urban Green. 82, 127896. https://doi.org/10.1016/j.ufug.2023.127896.
Seyfried, A., Steffen, B., Klingsch, W., Boltes, M., 2005. The fundamental diagram of pedestrian movement revisited. J. Stat. Mech. 2005, P10002. https://doi.org/10.1088/1742-5468/2005/10/p10002. P10002.
Shepard, D., 1968. A two-dimensional interpolation function for irregularly spaced data. In: Presented at the Proceedings of the 1968 23rd ACM National Conference. Association for Computing Machinery (ACM), New York, NY, USA, pp. 517–524. https://doi.org/10.1145/800186.810616.
Shu, D., Peng, Y., Zhang, Z., Shi, R., Wu, C., Gan, D., Li, X., 2024. Distance decay of urban Park visitation: roles of personal characteristics and visitation patterns. Forests 15, 1589. https://doi.org/10.3390/f15091589.
Slawsky, E.D., Hajat, A., Rhew, I.C., Russette, H., Semmens, E.O., Kaufman, J.D., Leary, C.S., Fitzpatrick, A.L., 2022. Neighborhood greenspace exposure as a protective factor in dementia risk among U.S. adults 75 years or older: a cohort study. Environ. Health 21, 14. https://doi.org/10.1186/s12940-022-00830-6.
Soncini, C., Chiari, A., Rothman, K.J., Martini, N., Cherubini, A., Despini, F., Costanzini, S., Girolamo, G.D., Tondelli, M., Vinceti, G., Zamboni, G., Teggi, S., Maffeis, G., Vinceti, M., Filippini, T., 2025. A two-dimensional interpolation function for irregularly spaced data. In: Presented at the Proceedings of the 1968 23rd ACM National Conference. Association for Computing Machinery (ACM), New York, NY, USA. https://doi.org/10.1159/000549445.
Spearman, C., 1904. The proof and measurement of association between two things. Am. J. Psychol. 15, 72–101. https://doi.org/10.2307/1412159.
Taylor, P.J., 1971. Distance transformation and distance decay functions. Geogr. Anal. 3, 221–238. https://doi.org/10.1111/j.1538-4632.1971.tb00364.x.
Teggi, S., Costanzini, S., Ghermandi, G., Malagoli, C., Vinceti, M., 2018. A GIS-based atmospheric dispersion model for pollutants emitted by complex source areas. Sci. Total Environ. 610–611, 175–190. https://doi.org/10.1016/j.scitotenv.2017.07.196.
Tian, Y., Jim, C.Y., Tao, Y., Shi, T., 2011. Landscape ecological assessment of green space fragmentation in Hong Kong. Urban For. Urban Green. 10, 79–86. https://doi.org/10.1016/j.ufug.2010.11.002.
Tucker, C.J., 1979. Red and photographic infrared Linear combinations for monitoring vegetation. Rem. Sens. Environ. 8, 127–150. https://doi.org/10.1016/0034-4257(79)90013-0.
Twohig-Bennett, C., Jones, A., 2018. The health benefits of the great outdoors: a systematic review and meta-analysis of greenspace exposure and health outcomes. Environ. Res. 166, 628–637. https://doi.org/10.1016/j.envres.2018.06.030.

U.S. Geological Survey (USGS), 2019a. Landsat 8 (L8) Data Users Handbook. NASA and U.S. Geological Survey, Sioux Falls, SD, USA.
U.S. Geological Survey (USGS), 2019b. Landsat 7 Science Data User's Handbook. U.S. Geological Survey, Sioux Falls, SD.
Villanueva-Durbán, N., Lorenzo-Sáez, E., Lerma-Arce, V., Coll-Aliaga, E., 2025. Evaluation of urban accessibility through geomarketing techniques: case study in Valencia (Spain). IJGI 14, 60. https://doi.org/10.3390/ijgi14020060.
Vinceti, M., Filippini, T., Violi, F., Rothman, K.J., Costanzini, S., Malagoli, C., Wise, L.A., Odone, A., Signorelli, C., Iacuzio, L., Arcolin, E., Mandrioli, J., Fini, N., Patti, F., Lo Fermo, S., Pietrini, V., Teggi, S., Ghermandi, G., Scillieri, R., Ledda, C., Mauceri, C., Sciacca, S., Fiore, M., Ferrante, M., 2017a. Pesticide exposure assessed through agricultural crop proximity and risk of amyotrophic lateral sclerosis. Environ. Health 16. https://doi.org/10.1186/s12940-017-0297-2.
Vinceti, M., Malagoli, C., Fabbi, S., Kheifets, L., Violi, F., Poli, M., Caldara, S., Sesti, D., Violanti, S., Zanichelli, P., Notari, B., Fava, R., Arena, A., Calzolari, R., Filippini, T., Iacuzio, L., Arcolin, E., Mandrioli, J., Fini, N., Odone, A., Signorelli, C., Patti, F., Zappia, M., Pietrini, V., Oleari, P., Teggi, S., Ghermandi, G., Dimartino, A., Ledda, C., Mauceri, C., Sciacca, S., Fiore, M., Ferrante, M., 2017b. Magnetic fields exposure from high-voltage power lines and risk of amyotrophic lateral sclerosis in two Italian populations. Amyotrophic Lateral Sclerosis and Frontotemporal Degeneration 18, 583–589. https://doi.org/10.1080/21678421.2017.1332078.
Weidmann, U., 1992. Transporttechnik der Fussgänger: Transporttechnische Eigenschaften des Fussgängerverkehrs, Literaturauswertung. ETH Zurich. https://doi.org/10.3929/ETHZ-A-000687810.
Więckowski, J., Sałabun, W., 2023. Sensitivity analysis approaches in multi-criteria decision analysis: a systematic review. Appl. Soft Comput. 148, 110915. https://doi.org/10.1016/j.asoc.2023.110915.
Wulder, M.A., Loveland, T.R., Roy, D.P., Crawford, C.J., Masek, J.G., Woodcock, C.E., Allen, R.G., Anderson, M.C., Belward, A.S., Cohen, W.B., Dwyer, J., Erb, A., Gao, F., Griffiths, P., Helder, D., Hermosilla, T., Hipple, J.D., Hostert, P., Hughes, M.J., Huntington, J., Johnson, D.M., Kennedy, R., Kilic, A., Li, Z., Lymburner, L., McCorkel, J., Pahlevan, N., Scambos, T.A., Schaaf, C., Schott, J.R., Sheng, Y., Storey, J., Vermote, E., Vogelmann, J., White, J.C., Wynne, R.H., Zhu, Z., 2019. Current status of landsat program, science, and applications. Rem. Sens. Environ. 225, 127–147. https://doi.org/10.1016/j.rse.2019.02.015.
Wulder, M.A., White, J.C., Loveland, T.R., Woodcock, C.E., Belward, A.S., Cohen, W.B., Fosnight, E.A., Shaw, J., Masek, J.G., Roy, D.P., 2016. The global landsat archive: status, consolidation, and direction. Rem. Sens. Environ. 185, 271–283. https://doi.org/10.1016/j.rse.2015.11.032.
Xu, Y., Yang, Y., Chen, X., Liu, Y., 2022. Bibliometric analysis of global NDVI research trends from 1985 to 2021. Remote Sens. 14, 3967. https://doi.org/10.3390/rs14163967.
Yan, K., Gao, Si, Yan, G., Ma, X., Chen, X., Zhu, P., Li, J., Gao, Sicong, Gastellu-Etchegorry, J.-P., Myneni, R.B., Wang, Q., 2025. A global systematic review of the remote sensing vegetation indices. Int. J. Appl. Earth Obs. Geoinf. 139, 104560. https://doi.org/10.1016/j.jag.2025.104560.
Yenisetty, P., Bahadure, P., 2020. Measuring accessibility to various ASFs from public transit using spatial distance measures in Indian cities. IJGI 9, 446. https://doi.org/10.3390/ijgi9070446.
Yuan, B., Zhou, L., Dang, X., Sun, D., Hu, F., Mu, H., 2021. Separate and combined effects of 3D building features and urban green space on land surface temperature. J. Environ. Manag. 295, 113116. https://doi.org/10.1016/j.jenvman.2021.113116.
Yuchi, W., Sbihi, H., Davies, H., Tamburic, L., Brauer, M., 2020. Road proximity, air pollution, noise, green space and neurologic disease incidence: a population-based cohort study. Environ. Health 19, 8. https://doi.org/10.1186/s12940-020-0565-4.
Zanaga, D., Van De Kerchove, R., De Keersmaecker, W., Souverijns, N., Brockmann, C., Quast, R., Wevers, J., Grosu, A., Paccini, A., Vergnaud, S., Cartus, O., Santoro, M., Fritz, S., Georgieva, I., Lesiv, M., Carter, S., Herold, M., Li, L., Tsendbazar, N.-E., Ramoino, F., Arino, O., 2021. ESA Worldcover 10 M 2020 v100. https://doi.org/10.5281/ZENODO.5571936.
Zhao, Q., Yu, L., Li, X., Peng, D., Zhang, Y., Gong, P., 2021. Progress and trends in the application of Google Earth and google Earth engine. Remote Sens. 13, 3778. https://doi.org/10.3390/rs13183778.